

Control of the bootstrap current in approximately quasi-axisymmetric magnetic fields

J.L. Velasco, I. Calvo, and J. M. García-Regaña
Laboratorio Nacional de Fusión, CIEMAT, 28040 Madrid, Spain
 (Dated: March 23, 2026)

Quasi-axisymmetric stellarators are the stellarator analogue of the axisymmetric tokamak, retaining many of its favorable confinement properties, its compactness and its relative coil simplicity, while avoiding its principal limitation, the need for an inductively driven plasma current. Despite these attractive physics properties, the development of quasi-axisymmetric configurations has been severely constrained by the absence of an experimentally validated divertor concept compatible with their large bootstrap current. In this Letter, approximately quasi-axisymmetric fields, complemented with piecewise omnigenous perturbations, are proposed as the basis for a new strategy towards a stellarator reactor that simultaneously achieves simple coil geometries, tokamak-like confinement properties and, through tailoring of the bootstrap current, compatibility with an island divertor. Implications for attaining a high bootstrap current fraction in tokamak devices are also discussed.

Magnetic confinement fusion aims to confine a hot plasma by means of strong magnetic fields that form nested toroidal flux surfaces. One of the central challenges is to limit transport processes across flux surfaces so that the plasma achieves the temperatures and densities required for fusion reactions to proceed efficiently [1].

The tokamak [2] has been the leading magnetic confinement concept because it combines a relatively simple geometry with excellent confinement properties. Its axisymmetry results in favorable neoclassical transport (the one associated with particle trajectories in an inhomogeneous magnetic field and collisions), and decades of experimental development have led to a relatively well-established route toward reactor-scale devices. However, despite these strengths, the tokamak suffers from intrinsic limitations. Its operation relies on a large, mainly inductive, plasma current, which enforces pulsed operation and makes the device vulnerable to current-driven instabilities and potentially disruptive events. This poses significant challenges for steady-state reactor operation. Strategies to mitigate these weaknesses include non-inductive current drive (e.g. [3]) and operation with a high bootstrap current fraction [4, 5]. Nevertheless, current drive displays degraded efficiency in a reactor-size device, and the bootstrap current, a self-generated current caused by neoclassical effects, is limited by the size of the plasma gradients. Stellarators [6] overcome these limitations by generating the confining magnetic field entirely through external coils. This facilitates steady-state operation and eliminates disruptions, but requires fully three-dimensional magnetic fields whose geometry must be carefully optimized to achieve acceptable transport [7].

In both tokamaks and stellarators, charged particles approximately follow the magnetic field lines, executing fast gyromotion around them. On time scales much longer than the gyroperiod, magnetic field inhomogeneities and curvature give rise to *drifts*, causing particles to slowly separate from individual field lines and, in particular, to move across flux surfaces. If the ratio between the particle energy \mathcal{E} and the magnetic moment μ is larger than the maximum value of the magnetic field strength $B = |\mathbf{B}|$ on the flux surface, particles are *pass-*

ing: their velocity component parallel to the magnetic field never vanishes, they explore the whole flux surface and remain, on average, tied to it. Particles with smaller \mathcal{E}/μ are *trapped*: they bounce back and forth between *bounce points*, where the parallel velocity vanishes, typically tracing banana-shaped trajectories in a small region of the flux surface. In axisymmetric tokamaks, the radial drift of these particles averages to zero; this is not the case of a unoptimized stellarator, which leads to unacceptably large transport of energy across flux surfaces.

All strategies for the optimization of stellarators with respect to neoclassical transport can be understood in terms of the second adiabatic invariant

$$J \equiv 2 \int_{l_{b_1}}^{l_{b_2}} dl \sqrt{2(\mathcal{E} - \mu B)}, \quad (1)$$

defined for trapped particles. Here, l is the arc-length along the field line, and l_{b_1} and l_{b_2} the bounce-point positions, defined as the points where $\mathcal{E}/\mu = B$. Ensuring that the contours of constant J are aligned with the flux surfaces, as in omnigenous fields [8], implies that the (orbit-averaged) radial drift of trapped particles is zero. As a consequence, in omnigenous fields, low collisionality transport is described by neoclassical coefficients proportional to the collisionality, as in a tokamak, rather than exhibiting the $1/\nu$ transport characteristic of a generic stellarator. In terms of the temperature, this leads to a neoclassical heat flux with a much less unfavorable scaling, proportional to $T^{1/2}$ instead of $T^{9/2}$, see e.g. [9].

The constraints that omnigenity imposes on the variation of B on the flux surface are best understood if the latter is parametrized using Boozer poloidal and toroidal angles, θ and ζ [10]. In these coordinates, $dl/d\theta = (B_\zeta/\iota + B_\theta)/B$, where $B_\theta = \mathbf{B} \cdot \mathbf{e}_\theta$, $B_\zeta = \mathbf{B} \cdot \mathbf{e}_\zeta$, and the rotational transform ι are flux-surface constants. It then becomes clear that the spatial dependence of the integrand of equation (1) is determined by $B(\theta, \zeta)$. In an axisymmetric tokamak, $B = B(\theta)$ guarantees that J is a flux-surface constant. Conversely, in quasisymmetric (QS) stellarators, a subset of omnigenous fields, this is achieved by making B depend on the angular position

parallelogram with $B = B_{\max}$ is $2w_1$. The toroidal extent of the one with $B = B_{\text{mid}}$ is $2(\pi/N_{fp} - w_1)$, N_{fp} being the number of field periods. The rotational transform

$$\iota = \frac{i_\theta \pi - w_2}{i_\zeta \pi / N_{fp} + t_1 w_2} \quad (2)$$

ensures that the top corners of any $B = B_{\max}$ parallelogram are connected by only two field lines with the bottom corners of another $B = B_{\max}$ parallelogram, with i_ζ and i_θ integer numbers and $i_\zeta 2\pi/N_{fp}$ and $i_\theta 2\pi$ the toroidal and poloidal distance between the centers of the connected parallelograms [31] (this expression is different than the one of [30], which, for reasons that will become clear later, is incompatible with a bootstrap reduction [38]). The fact that the $B = B_{\max}$ parallelogram is centered at $(\zeta, \theta) = (\pi/N_{fp}, \pi)$ ensures stellarator symmetry. Crucially, equation (2) does not contain w_1 .

From the point of view of radial transport, the phase space can be divided into four relevant types of orbits. Trapped particles with $B_{\min} < \mathcal{E}/\mu \leq B_{\text{mid}}$ (light blue) have their bounce points at $\theta = \pi \pm w_2$ and behave as in a QA field, with $J = J_0$. Conversely, trapped particles with $B_{\text{mid}} < \mathcal{E}/\mu \leq B_{\max}$ see a pwO field, and may have three different values of J : $J^{(\text{I})}$ (purple), $J^{(\text{II})}$ (orange) and $J^{(\text{III})} = J^{(\text{I})} + J^{(\text{II})}$ (green). This spatial distribution of J ensures tokamak-like radial neoclassical transport of the bulk species at low collisionality.

From the point of view of parallel transport, there are three relevant regions. The $B = B_{\text{mid}}$ region is labelled as region 1. Region 2 is a parallelogram with two sides of slope ι and two horizontal sides lying along the boundaries between $B = B_{\min}$ and $B = B_{\text{mid}}$. The remaining portion of the $B = B_{\min}$ area is labeled as region 3.

As explained in Appendix A, the bootstrap current of the magnetic field of figure 1 is zero if

$$\Delta_{\text{QA-pwO}} = 0, \quad (3)$$

where

$$\begin{aligned} \Delta_{\text{QA-pwO}} = & \frac{A_1}{(\iota - a_1)B_{\text{mid}}^2} \left(\hat{f}_t(B_{\text{mid}}, B_{\max}) - f_t \right) + \\ & \frac{A_2}{(\iota - a_1)B_{\text{min}}^2} \left(\hat{f}_t(B_{\min}, B_{\max}) - \hat{f}_t(B_{\min}, B_{\text{mid}}) \right) + \\ & \frac{A_2}{\iota B_{\text{min}}^2} \left(\hat{f}_t(B_{\min}, B_{\text{mid}}) - f_t \right) + \\ & \frac{A_3}{\iota B_{\text{min}}^2} \left(\hat{f}_t(B_{\min}, B_{\max}) - f_t \right). \quad (4) \end{aligned}$$

The quantities \hat{f}_t and f_t take $O(1)$ values, and A_i is the area in (θ, ζ) space of region i . The definitions of \hat{f}_t and f_t , and expressions for A_i are provided in Appendix B.

Equation (3) needs to be solved numerically. One of the solutions is $N_{fp} = 2$, $i_\zeta = 4$, $i_\theta = 1$, $\iota = 0.439$, $a_1 = 0.616$, $w_1 = 0.559\pi/N_{fp}$, $w_2 = 0.424\pi$, $B_{\min} = 0.9$ T, $B_{\text{mid}} = 1.024$ T, $B_{\max} = 1.1$ T. This solution, along with

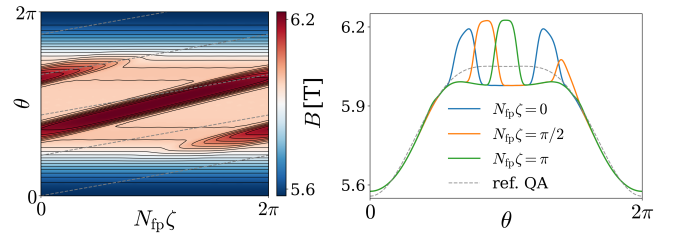


FIG. 2: B on the flux surface of a smooth nearly QA field with a pwO perturbation that reduces the bootstrap current.

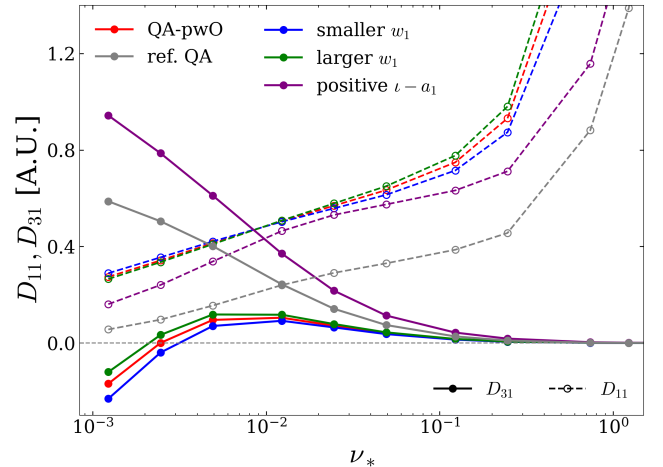


FIG. 3: Radial (D_{11}) and parallel (D_{31}) neoclassical transport coefficients as a function of the collisionality.

the discussion of this section, serves the purpose of illustrating key aspects required to achieve a reduced bootstrap current. B -contours of constant θ give a contribution to the bootstrap current with a definite sign (in a QA field, only this type of B -contours exist, giving a large bootstrap current comparable to that of the tokamak). In order to compensate for this, there must exist B -contours of constant $\theta - a_1\zeta$, with negative $\iota - a_1$. The relative areas of regions 1, 2 and 3, combined with the relative values of B , of ι and of $a_1 - \iota$ will determine whether the bootstrap current vanishes at low collisionality.

II. A SMOOTH NEARLY QA FIELD WITH REDUCED BOOTSTRAP CURRENT

Figure 2 shows the magnetic field strength of a model QA-pwO field, similar to that of figure 1 (so that its features can still be discussed in terms of quantities such as w_1 or a_1), but more realistic. The parameters describing $B(\theta, \zeta)$ are provided in Appendix C. Figure 2 (right) also depicts an exactly QA field that will be used for reference.

Figure 3 shows the level of parallel and radial transport of several QA-pwO magnetic fields. Specifically, the D_{11} and D_{31} neoclassical transport coefficients are computed with MONKES [39, 40] in the absence of radial elec-

tric field, as these coefficients encapsulate the dependence of neoclassical transport on the details of the magnetic configuration, see e.g. [9]. The main thesis of this work is proven correct: a pwO perturbation can significantly reduce the bootstrap current (with respect to a reference QA, compare red and gray) while keeping a low radial neoclassical transport. Specifically, at reactor-relevant collisionality, the bootstrap current can be made to vanish without causing the emergence of a $1/\nu$ regime for radial transport. Additionally, the QA-pwO cases with a smaller/larger value of w_1 (blue/green) illustrate some degree of control over the bootstrap current level. Finally, the case with positive $\iota - a_1$ (purple) shows that the bootstrap current can be increased, rather than reduced. This will be later discussed in the context of tokamak operation with a high bootstrap current fraction.

III. DISCUSSION

The result of section II opens a new pathway for the design of a stellarator reactor that may combine simple coil geometries, tokamak-like confinement properties, and compatibility with an island divertor. In this section we present a few preliminary analyses in this direction.

In figure 3, the QA-pwO field of figure 2 showed, at low collisionalities, a bootstrap level roughly an order of magnitude below a QA field. This is a reduction comparable to the that of the *standard* configuration of W7-X [9], which has been experimentally demonstrated to be compatible with an island divertor [29]. However, when scaled to a reactor scenario with higher temperatures, this level of bootstrap current may still be too high. Further optimization, in order to make D_{31} comparable to that of the high-mirror configuration of W7-X, could then be necessary [41, 42]. In order to assess this, we next give an order-of-magnitude estimate of the effect of the level of bootstrap current shown in figure 3.

We compute the bootstrap current profile of a reactor scenario, and use it to estimate the associated change in the rotational transform at the edge, $\Delta\iota$. Details on the calculation, including the plasma profiles and how the model fields (which are defined on a flux surface) are extrapolated to a whole volume are given in Appendix D. The results are shown in figure 4 as a function of the density and temperature at the core. Even if D_{31} is too large, the fact that it changes sign at low collisionality already offers a pathway for the reduction $\Delta\iota$ to acceptable levels. In particular, $\Delta\iota = 0$, required for an island divertor, can result from canceling a negative core contribution (where ν_* is lower) with a positive edge contribution.

The range of plasma profiles for which $\Delta\iota$ is small enough (the contours $\Delta\iota = \pm 0.02$ are highlighted in figure 4, as a rough indicator of the variation of ι that can be expected from other finite- β effects) is determined by the size of D_{31} at intermediate collisionalities. Although already smaller than in a QA stellarator, further reduction of D_{31} could make the range large enough for a safe

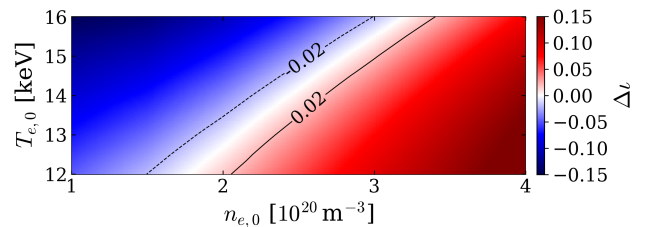


FIG. 4: Change in the rotational transform due to the bootstrap current in a reactor scenario for a model QA-pwO field.

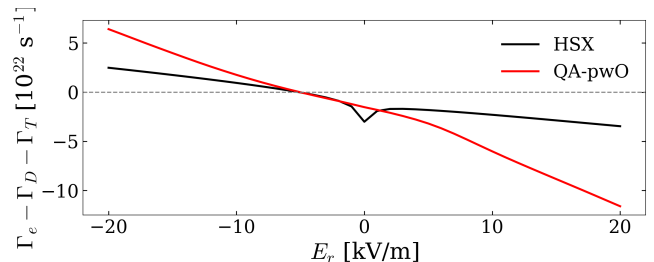


FIG. 5: Dependence of the radial charge current on the radial electric field E_r for $n_{e,0} = 4 \times 10^{20} \text{ m}^{-3}$ and $T_{e,0} = 12 \text{ keV}$.

operation of the island divertor.

The need for scenario development is not new in stellarators (QI candidates [24–26, 28, 43], for instance, rely for turbulence reduction on a relatively fine [44] control over of the density profile shape). Since the temporal evolution of the toroidal current is slower than the transport time scale [45], a relatively small (compared to a QA field) $\Delta\iota$ could perhaps be compensated by adjustments of the average density, or by current drive. In any case, further optimization of the (self-consistent [46, 47]) bootstrap current should undoubtedly be the next step.

The fields presented in this Letter can be argued to be approximately quasisymmetric. However, particles with $\mathcal{E}/\mu \lesssim B_{\text{max}}$ do experience $O(1)$ deviations from quasisymmetry, which casts doubts on the capability of such fields to sustain large flows (or equivalently, to be automatically ambipolar [48, 49]) or screen impurities. Since earlier analytical studies [48–50] are not directly applicable, we address the problem by means of a numerical comparison with the approximately quasisymmetric stellarator HSX scaled to reactor size, whose level of optimization has been experimentally proven to reduce radial transport and flow damping in the direction of symmetry [51, 52] (the behaviour of impurities, on the other hand, is qualitatively similar to that of a non-QS stellarator [53]). Figure 5 shows that the model QA-pwO field and HSX (at an intermediate radial position) meet the condition of automatic ambipolarity ($\Gamma_e - \Gamma_H - \Gamma_D = 0$ for any radial electric field, Γ_b being the neoclassical particle flux) to a similar extent (i.e. with a similar slope around the ambipolar E_r value). This property may be optimized in QA-pwO field by making the pwO region smaller, likely

in combination with a smaller value of $|\iota - a_1|$.

Some considerations on feasibility are in order. We note that, when a good level of quasisymmetry can not be achieved in a neoclassically optimized configuration (due e.g. to incompatibility with other design constraints), QA-pwO features appear to form naturally. This can be argued to be the case in NCSX (see section 8 of [31] and figures 5 and 6 of [9]), which displays a lower level of neoclassical transport than HSX despite showing (at the high-field side) much larger deviations from quasisymmetry. Earlier, some of the *spherical* stellarators developed by Moroz [18] already displayed “quasi-helical symmetry of B [...] in the inboard halves of the flux surfaces [and] quasi-toroidal symmetry [at] the outboard halves”. The theoretical framework presented in this Letter, combined with the existence of more efficient optimization tools, opens a promising route towards the stellarator reactor.

Finally, the results of this Letter extend beyond quasi-axisymmetric stellarators. The framework of section I can be straightforwardly extended to quasi-helically symmetric stellarators. Moreover, figure 3 has shown that the bootstrap current can be *increased*, for given plasma gradients, with respect to that of a $B = B(\theta)$ field. In tokamaks, carefully designed QS deviations from axisymmetry have been experimentally shown to constitute

a robust path for error field correction [54]. Similarly, piecewise omnigenous deviations from axisymmetry, if they could be produced without significant toroidal flow damping, could represent a viable strategy towards tokamak operation with a higher bootstrap current fraction.

Acknowledgments

This work has been carried out within the framework of the EUROfusion Consortium, funded by the European Union via the Euratom Research and Training Programme (Grant Agreement No 101052200 EUROfusion). Views and opinions expressed are however those of the author(s) only and do not necessarily reflect those of the European Union or the European Commission. Neither the European Union nor the European Commission can be held responsible for them. This research was supported by grants PID2021-123175NB-I00 and PID2024-155580B-I00, Ministerio de Ciencia, Innovación y Universidades, Spain. The authors are grateful to all the developers of the codes MONKES, Neotransp and SFINCS. Calculations for this work made use of computational resources at Xula (CIEMAT) and Raven (MPG).

-
- [1] J. D. Lawson, Proceedings of the Physical Society. Section B **70**, 6 (1957), URL <https://doi.org/10.1088/0370-1301/70/1/303>.
- [2] L. Arcimovich, G. Bobrovskij, E. Gorbunov, D. Ivanov, V. Kirillov, J. Kuznecov, S. Mirnov, M. Petrov, K. Razumova, V. Strelkov, et al., *Experiments in Tokamak Devices* (IAEA, 1969).
- [3] S. Freethy, L. Figini, S. Craig, M. Henderson, R. Sharma, T. Wilson, and the STEP team, Nuclear Fusion **64**, 126035 (2024), URL <https://doi.org/10.1088/1741-4326/ad7a8a>.
- [4] R. J. Goldston, S. H. Batha, R. H. Bulmer, D. N. Hill, A. W. Hyatt, S. C. Jardin, F. M. Levinton, S. M. Kaye, C. E. Kessel, E. A. Lazarus, et al., Plasma Physics and Controlled Fusion **36**, B213 (1994), URL <https://doi.org/10.1088/0741-3335/36/12B/018>.
- [5] S. Ding and A. M. Garofalo, Reviews of Modern Plasma Physics **7**, 4 (2022), URL <https://doi.org/10.1007/s41614-022-00106-z>.
- [6] L. Spitzer, The Physics of Fluids **1**, 253 (1958), <https://aip.scitation.org/doi/pdf/10.1063/1.1705883>, URL <https://aip.scitation.org/doi/abs/10.1063/1.1705883>.
- [7] P. Helander, C. D. Beidler, T. M. Bird, M. Drevlak, Y. Feng, R. Hatzky, F. Jenko, R. Kleiber, J. H. E. Proll, Y. Turkin, et al., Plasma Physics and Controlled Fusion **54**, 124009 (2012), URL <https://doi.org/10.1088/0741-3335/54/12/124009>.
- [8] L. S. Hall and B. McNamara, The Physics of Fluids **18**, 552 (1975), ISSN 0031-9171, URL <https://doi.org/10.1063/1.861189>.
- [9] C. D. Beidler, K. Allmaier, M. Y. Isaev, S. V. Kasilov, W. Kernbichler, G. O. Leitold, H. Maaßberg, D. R. Mikkelsen, S. Murakami, M. Schmidt, et al., Nuclear Fusion **51**, 076001 (2011), URL <http://stacks.iop.org/0029-5515/51/i=7/a=076001>.
- [10] A. H. Boozer, The Physics of Fluids **26**, 496 (1983), <https://aip.scitation.org/doi/pdf/10.1063/1.864166>, URL <https://aip.scitation.org/doi/abs/10.1063/1.864166>.
- [11] J. Nührenberg and R. Zille, Physics Letters A **129**, 113 (1988), ISSN 0375-9601, URL <https://www.sciencedirect.com/science/article/pii/0375960188900801>.
- [12] J. R. Cary and S. G. Shasharina, Physical Review Letters **78**, 674 (1997), URL <http://link.aps.org/doi/10.1103/PhysRevLett.78.674>.
- [13] F. I. Parra, I. Calvo, P. Helander, and M. Landreman, Nuclear Fusion **55**, 033005 (2015).
- [14] A. G. Peeters, Plasma Physics and Controlled Fusion **42**, B231 (2000), URL <http://stacks.iop.org/0741-3335/42/i=12B/a=318>.
- [15] P. Helander and J. Nührenberg, Plasma Physics and Controlled Fusion **51**, 055004 (2009), URL <https://dx.doi.org/10.1088/0741-3335/51/5/055004>.
- [16] M. Landreman and P. J. Catto, Physics of Plasmas **19**, 056103 (2012).
- [17] G. G. Plunk, Journal of Plasma Physics **86**, 905860409 (2020).
- [18] P. Moroz, Nuclear Fusion **38**, 795 (1998), URL <https://dx.doi.org/10.1088/0029-5515/38/6/302>.
- [19] S. A. Henneberg and G. G. Plunk, Phys. Rev. Res. **6**, L022052 (2024), URL <https://link.aps.org/doi/10.1103/PhysRevResearch.6.L022052>.

- [20] D. Gates, S. Aslam, B. Berzin, P. Bonfigliolo, A. Cote, D. Dudt, E. Flom, D. Fort, A. Koen, T. Kruger, et al., *Nuclear Fusion* **65**, 026052 (2025), URL <https://doi.org/10.1088/1741-4326/ada56c>.
- [21] J. W. Connor, *Plasma Physics* **15**, 765 (1973), URL <http://stacks.iop.org/0032-1028/15/i=8/a=003>.
- [22] H. Sugama, T.-H. Watanabe, M. Nunami, and S. Nishimura, *Physics of Plasmas* **18**, 082505 (2011), ISSN 1070-664X, URL <https://doi.org/10.1063/1.3624483>.
- [23] E. Sánchez, J. Velasco, I. Calvo, and S. Mulas, *Nuclear Fusion* **63**, 066037 (2023), URL <https://dx.doi.org/10.1088/1741-4326/accd82>.
- [24] A. G. Goodman, P. Xanthopoulos, G. G. Plunk, H. Smith, C. Nührenberg, C. D. Beidler, S. A. Henneberg, G. Roberg-Clark, M. Drevlak, and P. Helander, *PRX Energy* **3**, 023010 (2024), URL <https://link.aps.org/doi/10.1103/PRXEnergy.3.023010>.
- [25] C. Hegna, D. Anderson, E. Andrew, A. Ayilaran, A. Bader, T. Bohm, K. C. Mata, J. Canik, L. Carbaljal, A. Cerfon, et al., *Journal of Plasma Physics* **91**, E76 (2025).
- [26] J. Lion, J.-C. Anglès, L. Bonauer, A. Bañón Navarro, S. Cadena Ceron, R. Davies, M. Drevlak, N. Fopiani, J. Geiger, A. Goodman, et al., *Fusion Engineering and Design* **214**, 114868 (2025), ISSN 0920-3796, URL <https://www.sciencedirect.com/science/article/pii/S0920379625000705>.
- [27] C. P. Swanson, *Fusion Engineering and Design* (submitted), URL <https://arxiv.org/html/2512.08027v2>.
- [28] E. Sánchez, *Nuclear Fusion* (submitted), URL <https://arxiv.org/abs/2512.08825>.
- [29] T. S. Pedersen, R. König, M. Jakubowski, M. Krychowiak, D. Gradic, C. Killer, H. Niemann, T. Szepesi, U. Wenzel, A. Ali, et al., *Nuclear Fusion* **59**, 096014 (2019), URL <https://doi.org/10.1088/1741-4326/ab280f>.
- [30] J. L. Velasco, I. Calvo, F. J. Escoto, E. Sánchez, H. Thienpondt, and F. I. Parra, *Phys. Rev. Lett.* **133**, 185101 (2024), URL <https://link.aps.org/doi/10.1103/PhysRevLett.133.185101>.
- [31] J. Velasco, E. Sánchez, and I. Calvo, *Nuclear Fusion* **65**, 056012 (2025), URL <https://dx.doi.org/10.1088/1741-4326/adc4f6>.
- [32] I. Calvo, J. L. Velasco, P. Helander, and F. I. Parra, *Phys. Rev. E* **112**, L023201 (2025), URL <https://link.aps.org/doi/10.1103/PhysRevE.112.L023201>.
- [33] J L Velasco and *et al.*, arXiv:2603.12377 (2026).
- [34] V. Fernandez-Pacheco, <https://arxiv.org/abs/2601.14886> (2026).
- [35] H. Liu, G. Yu, C. Zhu, and G. Zhuang, <https://arxiv.org/abs/2502.09350> (2025).
- [36] H. Liu *et al.*, arXiv:2603.12139 (2026).
- [37] I. Calvo *et al.*, in preparation (2026).
- [38] F. J. Escoto, private communications (2025).
- [39] F. J. Escoto, J. L. Velasco, I. Calvo, M. Landreman, and F. I. Parra, *Nuclear Fusion* **64**, 076030 (2024), URL <https://dx.doi.org/10.1088/1741-4326/ad3fc9>.
- [40] F. Escoto, J. Velasco, I. Calvo, and E. Sánchez, *Nuclear Fusion* **65**, 036017 (2025), URL <https://dx.doi.org/10.1088/1741-4326/ada7e0>.
- [41] C. D. Beidler and the W7-X Team, *Nature* **596**, 221 (2021), URL <https://doi.org/10.1038/s41586-021-03687-w>.
- [42] C. Beidler, E. Harmeyer, F. Herrnegger, Y. Igitkhanov, A. Kendl, J. Kisslinger, Y. Kolesnichenko, V. Lutsenko, C. Nührenberg, I. Sidorenko, et al., *Nuclear Fusion* **41**, 1759 (2001), URL <https://dx.doi.org/10.1088/0029-5515/41/12/303>.
- [43] J. García-Regaña, I. Calvo, E. Sánchez, H. Thienpondt, J. Velasco, and J. Capitán, *Nuclear Fusion* **65**, 016036 (2024), URL <https://dx.doi.org/10.1088/1741-4326/ad86cb>.
- [44] S. Bannmann, in *30th IAEA Fusion Energy Conference* (2025).
- [45] *NRL plasma formulary* (Naval Research Laboratory, 2018), p. 20.
- [46] Z. Feng, D. A. Gates, S. A. Lazerson, M. Landreman, N. Pomphrey, and G. Fu, *Physics of Plasmas* **27**, 022502 (2020), ISSN 1070-664X, URL <https://doi.org/10.1063/1.5127948>.
- [47] M. Landreman, S. Buller, and M. Drevlak, *Physics of Plasmas* **29**, 082501 (2022), <https://doi.org/10.1063/5.0098166>, URL <https://doi.org/10.1063/5.0098166>.
- [48] I. Calvo, F. I. Parra, J. A. Alonso, and J L Velasco, *Plasma Physics and Controlled Fusion* **56**, 094003 (2014), URL <http://stacks.iop.org/0741-3335/56/i=9/a=094003>.
- [49] I. Calvo, F. I. Parra, J L Velasco, and J. A. Alonso, *Plasma Physics and Controlled Fusion* **57**, 014014 (2015), URL <http://stacks.iop.org/0741-3335/57/i=1/a=014014>.
- [50] I. Calvo, F. I. Parra, J L Velasco, and J. A. Alonso, *Plasma Physics and Controlled Fusion* **55**, 125014 (2013), URL <http://stacks.iop.org/0741-3335/55/i=12/a=125014>.
- [51] S. P. Gerhardt, J. N. Talmadge, J. M. Canik, and D. T. Anderson, *Phys. Rev. Lett.* **94**, 015002 (2005), URL <https://link.aps.org/doi/10.1103/PhysRevLett.94.015002>.
- [52] J. M. Canik, D. T. Anderson, F. S. B. Anderson, C. Clark, K. M. Likin, J. N. Talmadge, and K. Zhai, *Physics of Plasmas* **14**, 056107 (2007).
- [53] C. Swee, B. Geiger, R. Dux, S. T. A. Kumar, J. F. Castillo, A. Bader, and M. Gerard, *Plasma Physics and Controlled Fusion* **64**, 015008 (2021), URL <https://doi.org/10.1088/1361-6587/ac3965>.
- [54] J.-K. Park, S. M. Yang, N. C. Logan, Q. Hu, C. Zhu, M. C. Zarnstorff, R. Nazikian, C. Paz-Soldan, Y. M. Jeon, and W. H. Ko, *Phys. Rev. Lett.* **126**, 125001 (2021), URL <https://link.aps.org/doi/10.1103/PhysRevLett.126.125001>.
- [55] I. Calvo, F. I. Parra, J. L. Velasco, J. A. Alonso, and J. M. García-Regaña, *Nuclear Fusion* **58**, 124005 (2018), URL <http://stacks.iop.org/0029-5515/58/i=12/a=124005>.
- [56] P. Helander, F. I. Parra, and S. L. Newton, *Journal of Plasma Physics* **83**, 905830206 (2017).
- [57] H. M. Smith, IPP Greifswald (2020).
- [58] M. Landreman, H. Smith, A. Mollén, and P. Helander, *Physics of Plasmas* **21**, 042503 (2014), URL <http://scitation.aip.org/content/aip/journal/pop/21/4/10.1063/1.4870077>.

Appendix A: Calculation of the bootstrap current for a prototypical QA-pwO field

In order to streamline the calculation, in this appendix we follow the approach and notation of [56] for the computation of the bootstrap current in large aspect ratio stellarators at low collisionality, using a model collision operator. Then, we point out how, in the spirit of [32], one can derive the condition for zero bootstrap current for QA-pwO fields, and therefore obtain equation (3).

We write the bootstrap current as

$$\langle \mathbf{j}_{\parallel} \cdot \mathbf{B} \rangle = (f_s + \langle uB^2 \rangle)K, \quad (\text{A1})$$

where K depends on the plasma profile gradients and relatively trivial magnetic geometry properties. Here, u is calculated by solving the differential equation

$$\mathbf{B} \cdot \nabla u = -(\mathbf{B} \times \nabla s) \cdot \nabla B^{-2}, \quad (\text{A2})$$

with s the radial coordinate. If u is set to be zero in the region with $B = B_{\max}$, it is straightforward to show that

$$\begin{aligned} u_1 &= \frac{B_{\max}^{-2} - B_{\text{mid}}^{-2}}{\Psi'_t} \frac{a_1 B_{\theta} + B_{\zeta}}{\iota - a_1}, \\ u_2 - u_1 &= \frac{B_{\text{mid}}^{-2} - B_{\min}^{-2}}{\Psi'_t} \frac{B_{\zeta}}{\iota}, \\ u_3 &= \frac{B_{\max}^{-2} - B_{\min}^{-2}}{\Psi'_t} \frac{B_{\zeta}}{\iota}, \end{aligned} \quad (\text{A3})$$

where $2\pi\Psi_T$ is the toroidal flux through the last-closed flux surface and prime denotes radial derivative. f_s is defined as

$$f_s = \frac{3\langle B^2 \rangle}{4} \int_0^{B_{\max}^{-1}} d\lambda \frac{\lambda \langle g_4 \rangle}{\langle \sqrt{1 - \lambda B} \rangle}, \quad (\text{A4})$$

with g_4 obtained by solving

$$\mathbf{B} \cdot \nabla \left(\frac{g_4}{\xi} \right) = -(\mathbf{B} \times \nabla s) \cdot \nabla \xi^{-1}, \quad (\text{A5})$$

with $\xi = \sigma\sqrt{1 - \lambda B}$ and $\sigma = \pm 1$ the sign of the parallel velocity. If g_4 is set to be zero in the region with $B = B_{\max}$, it is straightforward to show that the values of g_4 in regions 1, 2 and 3 are given by

$$\begin{aligned} (g_4)_1 &= \left(1 - \frac{\xi_{\text{mid}}}{\xi_{\max}} \right) \frac{a_1 B_{\theta} + B_{\zeta}}{\iota - a_1}, \\ (g_4)_2 - (g_4)_1 \frac{\xi_{\min}}{\xi_{\text{mid}}} &= \left(1 - \frac{\xi_{\min}}{\xi_{\text{mid}}} \right) \frac{B_{\zeta}}{\iota}, \\ (g_4)_3 &= \left(1 - \frac{\xi_{\min}}{\xi_{\max}} \right) \frac{B_{\zeta}}{\iota}. \end{aligned} \quad (\text{A6})$$

It can be shown [15, 32] that the bootstrap current is zero for any plasma gradients if all the terms in equation (A1) that are proportional to B_{ζ} vanish. Computing (A1) using equations (A3) and (A6), this happens when equation (3) is fulfilled.

We finally note that, by setting $B_{\text{mid}} = B_{\min}$, one can recover the result of [32] (for the specific case in which two sides of the parallelogram are horizontal, $a_2 = 0$).

Appendix B: Definitions and explicit expressions for quantities in equation (4)

In section I, the quantities \hat{f}_t and f_t have been employed. Their definitions are:

$$\begin{aligned} \hat{f}_t(B_a, B_b) &= \frac{B_a^2}{B_b^2} - \\ &\frac{3\langle B^2 \rangle}{4} \int_0^{B_{\max}^{-1}} d\lambda \frac{\lambda}{\langle \sqrt{1 - \lambda B} \rangle} \frac{\sqrt{1 - \lambda B_a}}{\sqrt{1 - \lambda B_b}}, \end{aligned} \quad (\text{B1})$$

where $\langle \dots \rangle$ denotes flux-surface average, and

$$f_t = \hat{f}_t(B_a, B_a). \quad (\text{B2})$$

We note that f_t and $f_c = 1 - f_t$ are quantities usually employed in derivations that involve the solution of differential equations on the flux surface of stellarators, see e.g. [55].

Additionally, the areas in (θ, ζ) space of regions 1, 2, and 3, defined in Section I, can be expressed in terms of the parameters of the pwO piece of the QA-pwO field:

$$\begin{aligned} A_1 &= 4w_2(\pi/N_{fp} - w_1), \\ A_2 &= 4(\pi - w_2)(\pi/N_{fp} - w_1), \\ A_3 &= 4(\pi - w_2)w_1. \end{aligned} \quad (\text{B3})$$

Appendix C: pwO parametrization and Fourier spectrum of the magnetic field of figure 2

The pwO region of the magnetic field strength of figure 2 can be approximately be described by:

$$\begin{aligned} N_{fp} &= 2, \\ i_{\zeta} &= 4, \\ i_{\theta} &= 1, \\ w_1 &= 0.3\pi/N_{fp}, \\ w_2 &= 0.424\pi, \\ a_1 &= 0.616, \\ \iota &= 0.439. \end{aligned} \quad (\text{C1})$$

This is replaced by $w_1 = 0.35\pi/N_{fp}$ and $w_1 = 0.25\pi/N_{fp}$ for the cases with increased and reduced w_1 , respectively. Finally, for the case with positive $\iota - a_1$, we set $a_1 = 0.407$ and, following equation (2), $\iota = 0.6011$.

The Fourier spectrum of the magnetic field of figure 2 is

$$B(\theta, \zeta) = \sum_{m,n} B_{m,n} \cos(m\theta - nN_{fp}\zeta), \quad (\text{C2})$$

with the modes $|B_{mn}/B_{00}| > 10^{-4}$ T shown in table I.

m	n	B_{mn} [T]	B_{mn}/B_{00}
0	0	5.8704	1
1	0	-2.4602×10^{-1}	-4.1909×10^{-2}
2	0	-6.6680×10^{-2}	-1.1359×10^{-2}
3	1	4.3631×10^{-2}	7.4323×10^{-3}
4	1	-3.7288×10^{-2}	-6.3519×10^{-3}
2	1	-2.6972×10^{-2}	-4.5946×10^{-3}
6	2	2.4869×10^{-2}	4.2363×10^{-3}
7	2	-2.4715×10^{-2}	-4.2101×10^{-3}
5	1	1.4945×10^{-2}	2.5458×10^{-3}
3	0	1.3107×10^{-2}	2.2327×10^{-3}
5	2	-1.2736×10^{-2}	-2.1696×10^{-3}
8	2	1.2446×10^{-2}	2.1201×10^{-3}
10	3	-8.2574×10^{-3}	-1.4066×10^{-3}
9	3	7.1465×10^{-3}	1.2174×10^{-3}
4	0	6.6360×10^{-3}	1.1304×10^{-3}
16	5	5.2264×10^{-3}	8.9029×10^{-4}
1	1	5.0324×10^{-3}	8.5724×10^{-4}
11	3	5.0306×10^{-3}	8.5694×10^{-4}
17	5	-4.4105×10^{-3}	-7.5131×10^{-4}
0	1	4.3779×10^{-3}	7.4576×10^{-4}
7	1	-4.1999×10^{-3}	-7.1543×10^{-4}
15	5	-3.2780×10^{-3}	-5.5840×10^{-4}
8	3	-2.9249×10^{-3}	-4.9824×10^{-4}
19	6	2.8471×10^{-3}	4.8499×10^{-4}
20	6	-2.7946×10^{-3}	-4.7605×10^{-4}
3	2	2.7577×10^{-3}	4.6977×10^{-4}
10	2	-2.7518×10^{-3}	-4.6876×10^{-4}
13	4	2.7180×10^{-3}	4.6300×10^{-4}
1	-1	-2.6122×10^{-3}	-4.4499×10^{-4}
12	4	-2.0135×10^{-3}	-3.4299×10^{-4}
14	4	-1.9607×10^{-3}	-3.3399×10^{-4}
18	5	1.7303×10^{-3}	2.9476×10^{-4}
6	1	1.6914×10^{-3}	2.8812×10^{-4}
5	0	-1.6352×10^{-3}	-2.7855×10^{-4}
18	6	-1.4826×10^{-3}	-2.5255×10^{-4}
21	6	1.3834×10^{-3}	2.3565×10^{-4}
2	2	-1.0310×10^{-3}	-1.7563×10^{-4}
11	2	9.8789×10^{-4}	1.6828×10^{-4}
12	3	-8.9007×10^{-4}	-1.5162×10^{-4}
13	3	-8.3903×10^{-4}	-1.4293×10^{-4}
8	1	8.3863×10^{-4}	1.4286×10^{-4}
6	3	8.0607×10^{-4}	1.3731×10^{-4}
4	2	7.7581×10^{-4}	1.3216×10^{-4}
26	8	7.1962×10^{-4}	1.2258×10^{-4}
14	5	6.4289×10^{-4}	1.0951×10^{-4}
9	1	6.3812×10^{-4}	1.0870×10^{-4}
11	4	6.1547×10^{-4}	1.0484×10^{-4}
9	2	-6.1488×10^{-4}	-1.0474×10^{-4}

TABLE I: Fourier modes of the field of figure 2.

Appendix D: Reactor scenario

In this section, we describe the steps required to produce reactor-relevant neoclassical calculations out of model fields $B_{\text{QApwO}}(\theta, \zeta)$ defined on a flux surface. We will use $0 \leq s \leq 1$, proportional to the toroidal flux, as the radial coordinate.

First, inspired by [34], we extrapolate radially the model fields

$$B(s, \theta, \zeta) = \sum_{m,n} B_{m,n}(s) \cos(m\theta - nN_{fp}\zeta), \quad (\text{D1})$$

$$B_{m,n}(s) = B_{m,n}^{(\text{QApwO})} \times \begin{cases} \left(\frac{s}{s_0}\right)^{m/2}, & s < s_0, \\ \left(\frac{s}{s_0}\right)^{1/2}, & s \geq s_0, \end{cases} \quad (\text{D2})$$

$$B_{\text{QApwO}}(\theta, \zeta) = \sum_{m,n} B_{m,n}^{(\text{QApwO})} \cos(m\theta - nN_{fp}\zeta) \quad (\text{D3})$$

with $s_0 = 0.15$. Then, all the configurations are scaled to a major radius $R = 18.5$ m, and an on-axis magnetic field strength $B_{\text{axis}} = 5.5$ T (for the model fields, this is done by setting $B_{0,0}^{(\text{QApwO})} = B_{\text{axis}}$ and $B_\zeta = RB_{\text{axis}}$).

The neoclassical code **MONKES** is able to compute the neoclassical transport coefficients [9]. Convolution (including momentum conservation) of these coefficients to compute the neoclassical radial fluxes and parallel flows for a given set of plasma profiles is provided by the suite **Neotransp** [57] (some calculations were later repeated with **SFINCS** [58]). We consider a deuterium-tritium plasma with density and temperature [47]

$$n_b(s) = n_{b,0}(1 - s^5), \quad T_b(s) = T_{b,0}(1 - s), \quad (\text{D4})$$

with $n_{e,0} = 2n_{D,0} = 2n_{T,0}$ and $T_{e,0} = T_{D,0} = T_{T,0}$. Once the total bootstrap current is computed, the change in ι , shown in Figure 4, is estimated as

$$\Delta\iota(s) = \frac{\mu_0 R}{2sB_{\text{axis}}^2} \int_0^s \langle j_{\parallel} \cdot B \rangle(s') ds', \quad (\text{D5})$$

where μ_0 is the vacuum permeability.

For figure 5, we set $n_{e,0} = 4 \times 10^{20} \text{ m}^{-3}$ and $T_{e,0} = 12$ keV and perform the calculation at $s = s_0$.